New method for the determination of photoabsorption from transmittance measurements in the extreme ultraviolet

Franck Delmotte, Catherine Burcklen, Jennifer Alameda, Farhad Salmassi, Eric Gullikson, Regina Soufli

Research Article | Vol. 30, No. 13 / 20 Jun 2022 / Optics Express 23771
Optics EXPRESS

New method for the determination of photoabsorption from transmittance measurements in the extreme ultraviolet

FRANCK DELMOTTE,[1,*] CATHERINE BURCKLEN,[2] JENNIFER ALAMEDA,[2] FARHAD SALMASSI,[3] ERIC GULLIKSON,[3] AND REGINA SOUFLI[2]

[1] *Université Paris-Saclay, Institut d'Optique Graduate School, CNRS, Laboratoire Charles Fabry, 91127, Palaiseau, France*
[2] *Lawrence Livermore National Laboratory, 7000 East Avenue, Livermore, California 94550, USA*
[3] *Lawrence Berkeley National Laboratory, 1 Cyclotron Rd., Berkeley, California 94720, USA*
[*] *franck.delmotte@institutoptique.fr*

Abstract: We have developed a new method for the determination of photoabsorption at extreme ultraviolet wavelengths longer than 20 nm, where reliable refractive index values are sparse or non-existent. Our method overcomes the obstacle of multiple reflections that occur inside thin films in this spectral range, which up until now has prevented the accurate determination of photoabsorption from transmittance measurements. We have derived a mathematical expression that is independent of internal reflection amplitudes, while taking advantage of the transmittance oscillations stemming from such reflections. The method is validated on measurements of aluminum thin films. This advance will enable accurate refractive index values for many important materials for optical instrumentation, thus facilitating high-priority research on topics including coherent light sources, planetary and solar physics, and semiconductor manufacturing.

1. Introduction

The large discrepancies found between simulations and experimental data from optical instruments in the wavelength range 20–80 nm has been a long-standing issue in the scientific community and it has been traced to the lack of reliable refractive index values [1–6]. This problem is hindering progress in fields that are addressing important questions and challenges of our time: from cutting-edge physics, to exoplanet habitability, to energy security. The 20–80 nm portion of the Extreme Ultraviolet (EUV) spectrum contains atomic resonances from numerous elements and is central to several science and technology fields. The prominence of novel light sources in this spectral range (high-harmonic generation, synchrotrons, tabletop EUV sources and free-electron lasers) demands highly customized, complex optical instrumentation [7]. Applications include imaging, spectrometry and microscopy for plasma physics, astrophysics, solar and planetary physics, semiconductor manufacturing, nanoelectronic devices, attosecond science, synchrotron and free-electron laser (FEL) science [2,8–13]. Instrument design, in-band and out-of-band calibration and data analysis require accurate knowledge of the refractive index of the materials that compose the instrument optics (filters, mirrors, gratings, polarizers, detectors). Yet, EUV refractive index values are sparse and often unreliable: experimental data from different authors can differ by a factor of 10; the lack is notable at wavelengths longer than 20 nm and especially pronounced above 40 nm [5,6,14–18]. This is due to EUV-specific challenges, including materials sensitivity to surface roughness, oxidation and contamination, as well as the presence of multiple reflections within thin films (Fig. 1), that are preventing the accurate determination of the refractive index. The resulting discrepancies between as-designed and experimental instrument performance are preventing urgently needed research in the long-wavelength portion of the EUV

#461333 https://doi.org/10.1364/OE.461333
Journal © 2022 Received 17 Apr 2022; revised 18 May 2022; accepted 18 May 2022; published 15 Jun 2022

Optics EXPRESS

spectral range. One example from climate and planetary science is the question of how planets lose their atmosphere, which is related to planet habitability, a priority topic in both the European Astrobiology Roadmap and the US National Academies' 2020s decadal survey in Astronomy and Astrophysics [19]. This question is intricately linked to atmospheric heating and ionization occurring within the 20–80 nm wavelength region [20,21]. Currently, there are no consistent refractive index values to design and build space instruments to address this question. Another example is EUV solar physics: space-borne telescopes such as the Solar Dynamics Observatory, Solar Orbiter and the GOES satellites [10–13] aim to enhance our understanding of the Sun's plasma and magnetic field and their effects on Earth, including space weather phenomena such as solar flares and coronal mass ejections. Data analysis from these instruments is often hindered by the lack of accurate refractive index values [2,18]. A third example with implications in worldwide economy and security is optical instrumentation and metrology for semiconductor manufacturing, which requires precise knowledge of materials properties in this spectral region. It should be noted that the wavelength range 20-80 nm corresponds to binding energies of the outermost electrons in matter and sufficient predictive models for the refractive index in this spectral region do not exist.

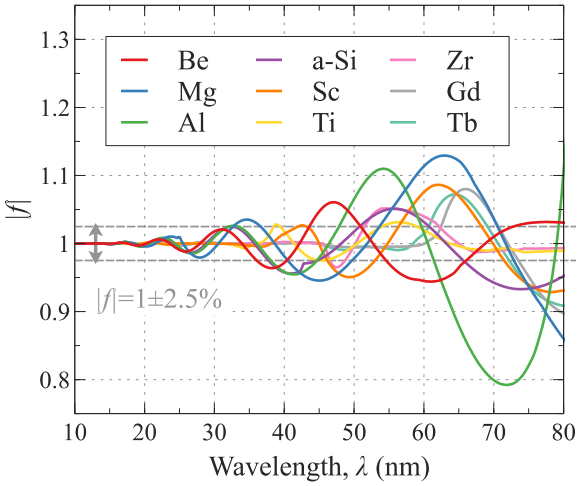

Fig. 1. Multiple reflection coefficient ($|f|$) calculated for various materials (25 nm thick free-standing films capped with a 5.5 nm C layer on each side). If multiple reflections are negligible, $|f|$ equals 1. If $|f|$ is outside the limits of $1 \pm 2.5\%$ (indicated as dashed lines), the transmittance T will be affected by more than ±5% by multiple reflections. See Section 2 for theoretical derivations and discussion of $|f|$ and T. The references used for the optical constants values of each material are: Be [14,15,33], Mg [33,34], Al [32,35], amorphous Si [14,15,33], Sc [36,37], Ti [14,15,31,38], Zr [15,38], Gd [30], and Tb [39].

The EUV refractive index (n) is a complex number given by the expression:

$$n = 1 - \delta + i\beta \tag{1}$$

where 1-δ is associated with the material dispersion, β is associated with the photoabsorption and (δ, β) are known as the "optical constants". In earlier work [22–30], a methodology has been established, based on measurements of the transmittance through a series of free-standing thin foils (in the 15 - 1000 nm thickness range), as one of the most reliable techniques for the determination of photoabsorption in the EUV/soft x-ray. This methodology overcomes most of the above-mentioned difficulties: it is relatively insensitive to roughness, allows the inclusion of capping layers (to prevent contamination of the material under study) and normalizes out their

Optics EXPRESS

effect in the analysis of the data. According to this method, the transmittance $T(\lambda)$ of a thin film sample at a wavelength λ can be expressed by a simple function of the film thickness d and the wavelength-dependent absorptive portion β of its refractive index:

$$T(\lambda) \approx T_0 \exp(-4\pi\beta d/\lambda) \tag{2}$$

β can be determined using a set of several films with different thicknesses, by fitting the measured transmittance as a function of film thickness at a given wavelength λ. The dispersive portion (1-δ) of the refractive index n can then be determined via the Kramers-Krönig relations [14,25–30]. However, Eq. (2) is valid only when multiple reflections inside the film structure are negligible, which is true only for the shorter wavelengths within the EUV spectrum [31]. This is illustrated in Fig. 1, where examples of important materials for optical instrumentation (Be, Mg, Al, amorphous Si, Sc, Ti, Zr, Gd, Tb, with optical constants obtained from Refs. 14, 15 and 30–39) are shown to produce significant multiple reflections in the wavelength range 20-80 nm. For instance, the absorption β of Al can be measured accurately via Eq. (2) only for wavelengths below 20 nm. At wavelengths longer than 20 nm, an Al thin film is highly transparent and yields strong multiple reflections at the interfaces with its surrounding media (air, oxide or capping layer), creating oscillations in the transmittance curves [22,40] and essentially preventing the determination of meaningful values for β from Eq. (2). We will be discussing in more detail Fig. 1 and the equation used to calculate the multiple reflection coefficient f in Sections 2 and 4 of this manuscript. In the literature, other methods have been proposed to determine both δ and β by fitting reflectance or ellipsometry data, but such data in the EUV spectral range are extremely sensitive to surface roughness, oxidation and contamination; although these properties can be measured independently or included in the fitting parameters, their presence complicates the fitting process and increases the uncertainty of the determined optical constant values [35,38,41–44]. The use of in-situ, ultra-high vacuum equipment may limit oxidation and contamination, but such measurements are much more complicated, usually available only on a restricted wavelength range and the spectral resolution is limited [37,41,43]. Some interesting interferometry-based methods have also been demonstrated, but their applicability at the longer EUV wavelengths, as well as their spectral resolution, are limited [45,46].

This paper proposes and validates a new method based on transmittance data that can overcome the obstacle of multiple reflections, thus enabling the accurate determination of photoabsorption (and ultimately, of the optical constants) for any thin film material in the long-wavelength portion of the EUV spectral range. The experimental validation of the new methodology is done by determining the photoabsorption of Al in the 20–72 nm wavelength region, via transmittance measurements on five free-standing C/Al/C thin films. This breakthrough will enable the design and implementation of EUV instrumentation and the accurate analysis of EUV data in this important but rather inaccessible region of the spectrum.

2. Theoretical development

To overcome the problem of multiple reflections discussed above, we propose a novel analysis technique of transmittance data: as will be shown below, we have conceived a transmittance function that is independent of the internal reflection coefficients in the film structure under study. At the same time, the function is taking advantage of the multiple reflections in the EUV range. It relies on the measurement of the oscillation local maxima (*Tmax*) and minima (*Tmin*) in the transmittance vs. wavelength plots and ultimately produces a simplified expression that is proportional to the right side of Eq. (2).

We consider the general case of a homogenous medium (M) embedded between two structures (B and C) with vacuum at the outside (see Fig. 2). The incident radiation arrives at normal incidence on the C structure. The M medium has a thickness d_M and a complex refractive index n_M. B and C media can represent homogenous base and capping layers or more complex thin

Optics EXPRESS

film stacks. Uspenskii et al. have demonstrated [31] that the total transmission of such a structure can be expressed with the following equation:

$$T(\lambda) = |t_C|^2 |t_B|^2 \, |f \; exp(i \, D_M)|^2 \tag{3}$$

t_C and t_B represent respectively the complex transmission amplitudes of the V/C/M and M/B/V structures (where M is considered as a semi-infinite medium and V represents the vacuum). $D_M = 2\,\pi\, n_M\, d_M\, /\lambda$ accounts for the propagation of the radiation through the M medium.

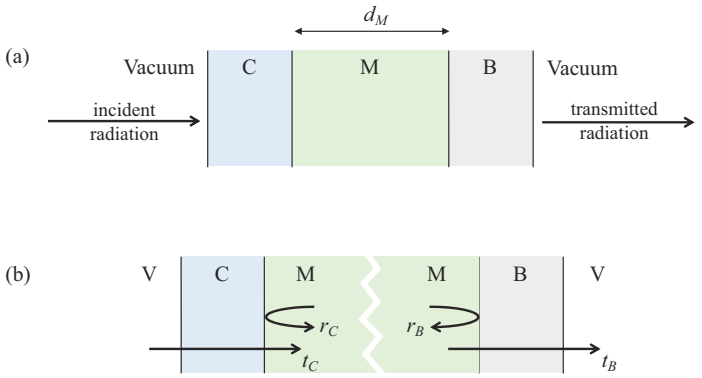

Fig. 2. **(a)** Schematic of the thin film layer structure. **(b)** Representation of the transmission (t_C, t_B) and reflection (r_C, r_B) coefficients used in the calculation of the total transmittance; the white zigzag line accounts for the fact that M is considered as a semi-infinite medium in the calculation of t_C, t_B, r_C and r_B.

The f factor accounts for the multiple reflections within the M media:

$$f = [1 - r_C r_B \exp(2i \, D_M)]^{-1} \tag{4}$$

r_C and r_B represent respectively the complex reflection amplitudes of the M/C/V and M/B/V structures (see Fig. 2). The multiple reflection coefficient $|f|$ for several relevant materials is plotted in Fig. 1. It is important to notice in Eq. (4) and Fig. 1 that multiple reflections become significant only if the reflection amplitudes r_C and r_B are not negligible: that occurs only for wavelengths longer than 25 nm for Al and Mg and longer than 35 nm for other materials. These wavelengths are typically longer than the outermost electronic absorption edge for each material. Therefore, we do not expect any absorption edges or related absorption fine structure in the spectral region of applicability of this method. This will be elaborated further in Sections 4 and 5, where more details on the implementation of the new method are discussed.

In the following, we consider the case when the media B and C are identical. Thus, naming φ the phase of r_C, we can write:

$$r_C = r_B = |r_C| \exp(i\varphi) \tag{5}$$

In addition, we use D' and D'' respectively as the real and imaginary parts of D_M:

$$D_M = D' + i \, D'' \tag{6}$$

By introducing Eqs. (4-6) in Eq. (3), a term $\cos(2D'+2\varphi)$ appears, which is related to the oscillations due to multiple reflections in $T(\lambda)$. The local maxima (*Tmax*) and minima (*Tmin*) of the transmittance oscillations correspond to $\cos(2D'+2\varphi)$ being equal to +1 and -1 respectively,

Optics EXPRESS

therefore:

$$Tmax = |t_C|^2|t_B|^2\exp(-2D'')[1 - 2|r_C|^2\exp(-2D'')]^{-2} \quad (7)$$

$$Tmin = |t_C|^2|t_B|^2\exp(-2D'')[1 + 2|r_C|^2\exp(-2D'')]^{-2} \quad (8)$$

We then define the quantity Σ below

$$\Sigma = \left(\frac{1}{\sqrt{Tmax}} + \frac{1}{\sqrt{Tmin}}\right)^{-2} = \Sigma_0\exp(-2D'') = \Sigma_0\exp(-4\pi\beta d_M/\lambda) \quad (9)$$

with $\Sigma_0 = \frac{|t_C|^2|t_B|^2}{4}$ and n_M =1-δ+iβ.

Plotting Σ as a function of thickness d for a given wavelength λ allows to determine β. We emphasize that the mathematical expression for Σ in Eq. (9) is especially designed to lead to a simplified exponential function that is independent of the internal reflection amplitude $|r_C|$, which is a unique, original and enabling component in our approach. Notice also that Eq. (9) normalizes out overlayers (Σ_0) in an analogous manner that T_0 does in the regular transmittance method of Eq. (2).

Earlier, another concept involving analysis of transmittance local maxima and minima was employed in the visible spectral range for the determination of refractive index [47]. The method discussed in this manuscript is fundamentally different than the approach in Ref. 47, for the following reasons: (i) Ref. 47 is based on transmittance measurements of a single sample on a semi-infinite substrate, under the assumption that the sample is fully transparent in a portion of the visible spectrum and that the presence of any overlayers on the sample surface (oxides, impurities) is insignificant. This scheme cannot work in the EUV range, due to the very high absorption of materials. In EUV transmittance measurements, films need to be free-standing or supported by a thin membrane. Furthermore, any oxide/contamination layers will significantly affect the EUV transmittance, therefore they need to be taken into account or prevented by protection layers. Finally, the need to normalize out any oxidation or protection layers from the EUV data requires measurements on multiple film thicknesses. All these elements result in a completely different layer structure and mathematical derivation. (ii) Differences between dispersion (1-δ) and absorption (β) are much more pronounced in the visible range than in the EUV and absorption in the visible is very low. As a result, transmittance oscillations (fringes) in the visible range are much more pronounced than in the EUV spectral range. Moreover, the effect of roughness/interdiffusion between layer interfaces is much more pronounced in EUV and could lead to a further dampening of the EUV fringe amplitude. Until our work, it was not clear if the number and quality of the fringes produced from films of different thicknesses would be sufficient to employ such fringes in quantitative analysis of transmittance data in the EUV.

3. Sample preparation and transmittance measurements

Five C/Al/C films were deposited at LLNL by Direct Current (DC) magnetron sputtering, on photoresist-coated Si wafer substrates. Each film had a different Al thickness (see Fig. 3). The thicknesses of the Al films were chosen so as to cover the widest possible range of transmittance values, in the wavelength range of interest. The thickness of each C layer was 5.5 nm on all samples. The C layers were added to protect each side of the Al film from oxidation, which in Al can be extensive and can complicate the measurements and data analysis. The effect of these C layers in the overall transmittance of the C/Al/C samples is represented by the quantity T_0 ("regular" method, Eq. (2)) and Σ_0 (new method, Eq. (9)) and it normalizes out of the data, as long as the C layer thickness is the same for all the films measured. The C and Al thickness values were verified at LLNL with an estimated accuracy better than 1%, by fitting reflectance vs. angle data obtained on the C/Al/C samples at 8.048 keV. Rutherford backscattering spectroscopy (performed at Eurofins EAG, Sunnyvale, California) was used to determine the purity of the

Optics EXPRESS

films: it revealed that the Al layers contain less than 30 ppm (atomic concentration) of Ta; no other contaminants were detectable. The C/Al/C films were removed from their substrates and mounted as free-standing films at the Center for X-ray Optics (CXRO) at Lawrence Berkeley National Laboratory (LBNL), using a method that has been discussed earlier [28]. The purity of the films against contaminants such as oxygen and photoresist residue from the removal/mounting process, was verified by transmittance measurements (not shown here) at beamline 6.3.2 of the Advanced Light Source (ALS) synchrotron at LBNL, around the carbon and oxygen K edge spectral regions, using a procedure discussed in Ref. 28.

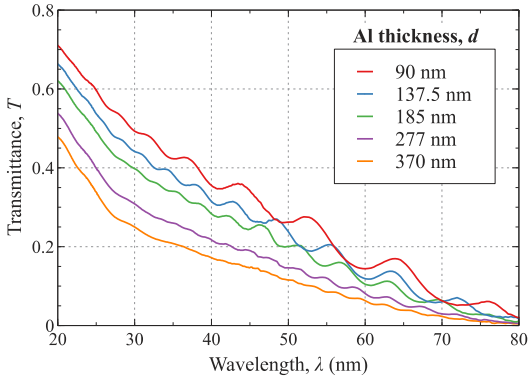

Fig. 3. Measured transmittance on five C/Al/C samples. The C cap layers are 5.5 nm thick for all samples. The thickness of Al varies from 90 nm to 370 nm (see legend).

For the determination of Al photoabsorption, transmittance measurements in the wavelength region 20–80 nm were performed on the five C/Al/C samples at beamline 6.3.2 and the results are shown in Fig. 3. Transmittance data were obtained in steps of 0.05 nm at wavelengths $\lambda < 25$ nm, 0.17 nm for 25 nm $< \lambda <$ 45 nm and 0.35 nm for $\lambda >$ 45 nm. The oscillations in transmittance caused by multiple reflections inside the C/Al/C films are evident in the data in Fig. 3.

4. Application of the new method on transmittance data

For each transmittance curve in Fig. 3, we apply the following procedure in order to determine the $Tmax(\lambda)$ and $Tmin(\lambda)$ of the measured $T(\lambda)$ data :

(i) Differentiate $[T(\lambda)]$ followed by smoothening (see Fig. 4(a)).

(ii) Determine the halfway point in-between each maximum and minimum of the derivative, which gives the wavelength λ_i for which $T(\lambda)$ reaches $Tmax$ (red crosses in Fig. 4(a)).

(iii) Determine the halfway point in-between each minimum and maximum of the derivative, which gives the wavelength λ_j for which $T(\lambda)$ reaches $Tmin$ (black crosses in Fig. 4(a)).

(iv) Interpolate the $T(\lambda_i)$ (resp. $T(\lambda_j)$) points with a cubic spline function in order to obtain $Tmax(\lambda)$ (resp. $Tmin(\lambda)$).

(v) If $Tmax(\lambda)$ (resp. $Tmin(\lambda)$) crosses $T(\lambda)$, refine the values of λ_i and λ_j by choosing the middle of the segment underlying (resp. overlying) $T(\lambda)$ (see Ref. 48) and return to step (iv).

This procedure and the resulting transmittance "envelopes" constructed from $Tmax(\lambda)$ and $Tmin(\lambda)$ data, are illustrated in Fig. 4 in the case of the 137.5 nm thick Al sample.

Optics EXPRESS

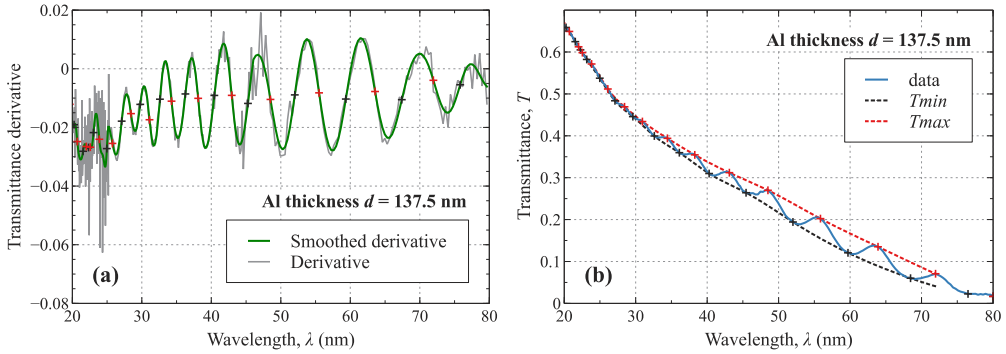

Fig. 4. (a) Derivative of the transmittance vs. wavelength and (b) upper (dash red line) and lower (dash black line) envelopes of transmittance vs. wavelength for an Al sample with 137.5 nm thickness.

Figure 5(a) shows the measured transmittance plotted on a logarithmic axis as a function of the Al thickness for several wavelengths in-between 20 nm and 70 nm. Due to the presence of multiple interferences, which generate oscillations in the $T(\lambda)$ data as shown in Fig. 3, most of the points are not aligned i.e. Equation (2) is no longer valid in this case, as was discussed in Section 1. It is interesting to notice that for specific wavelengths (e.g. 40 nm or 60 nm in Fig. 5(a)), points may align by coincidence. This is due to the fact that the $T(\lambda)$ oscillations for the 5 Al samples used in the measurements are almost in phase at these specific wavelengths (e.g. at 40 nm, all $T(\lambda)$ values present a minimum). However, even in the case where the points align, the slope is wrong and thus the photoabsorption coefficient deduced from these data would be erroneous. Moreover, due to the effort required to make the self-supported samples and to measure them on a wide transmittance range, the number of samples is usually limited to 2 or 3 different thickness values, which would increase the error in the determination of the slope.

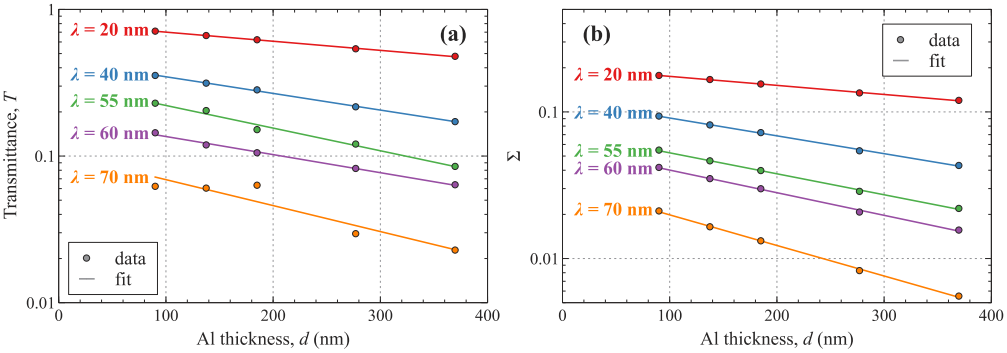

Fig. 5. **(a)** Transmittance, T and **(b)** Σ, plotted on a logarithmic axis, versus Al thickness for 5 C/Al/C films at different wavelengths. Dots represent experimental data and lines are the exponential fit of the data.

We have plotted in Fig. 5(b) the values of Σ plotted on a logarithmic axis, obtained from the transmittance data in Fig. 3 with the new method of (Eq. (9)) as a function of the Al thickness. The exponential fits of each data set (see Eq. (9)) are plotted as straight lines. For a given wavelength λ_k, the photoabsorption coefficient $\beta(\lambda_k)$ is given by the slope of the fit (equal to $-4\pi\beta(\lambda_k)/\lambda_k$) and the intercept defines the value of $\Sigma_0(\lambda_k)$. The dramatic improvement in the alignment of the data points in Fig. 5(b) compared to 5(a), is evident. We also calculated the

Optics EXPRESS

coefficient of determination (defined as the square of the Pearson correlation coefficient) for each fit from 20 nm to 72 nm wavelengths. This factor is higher than 0.998 (with 1 corresponding to a perfect agreement between fit and data) for most of the fits in this wavelength range, except at 45 nm to 53.5 nm where it is in the range 0.996 to 0.998. These lower values correspond to wavelengths where the experimental determination of *Tmax* and *Tmin* was less accurate due to lower photon flux leading to increased noise in the transmittance data (see Fig. 3). These high values of coefficient of determination confirm that the method used to determine $Tmax(\lambda)$ and $Tmin(\lambda)$ from experimental data is accurate, even for the thicker samples for which the oscillations are faint.

Figure 6 shows the photoabsorption coefficient β of Al deduced from the present work using the new method (Eq. (9)) and the regular method (Eq. (2)). It is interesting to notice that there is a very good overlap between the photoabsorption values derived with the regular method and the new Σ method at wavelengths below 25 nm, where the effect of multiple reflections is very small (as predicted in Eq. (4) and Fig. 1). For wavelengths above 25 nm however, the photoabsorption values calculated with the regular method start to exhibit oscillatory patterns and to deviate from the new method, with differences as high as 25% around 65 nm. Note that the oscillatory patterns obtained with the regular method get even worse if we reduce the number of Al samples used in the calculation. For example, by using the 3 thinnest samples from Fig. 3 (instead of all 5 samples), we obtain differences in β as high as 90% compared to the new method. We plotted also in Fig. 6 the currently available tabulated values of Al photoabsorption coefficients for comparison: (i) a compilation from Shiles [32,33] based on experimental data from Ditchburn [22], and (ii) β calculated from the imaginary part of the atomic scattering factors tabulated on the CXRO database [15] using an Al density of 2.7 g/cm^3. The CXRO database is the worldwide reference for EUV optical constants values. It contains a compilation of experimentally determined photoabsorption based on the Henke Tables [14]. In the case of Al, the photoabsorption has been updated with experimental data by Gullikson [24] in the wavelength region 17–41 nm.

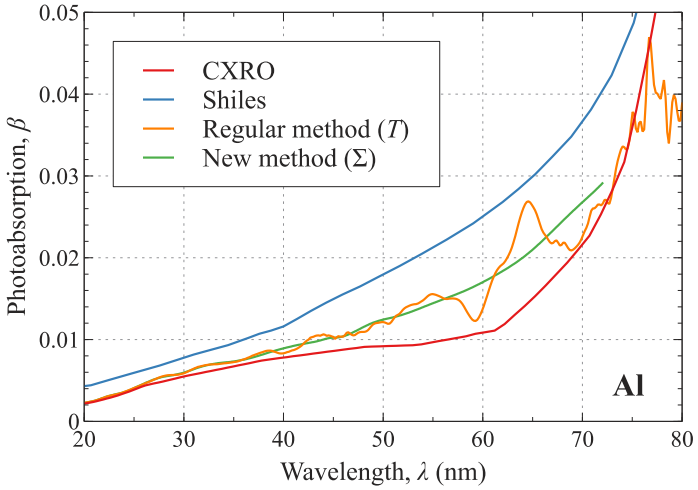

Fig. 6. Photoabsorption β of aluminum thin films derived with the new Σ method (Eq. (9)) and the regular transmittance method (Eq. (2)). Currently available tabulated data are also plotted for comparison: CXRO [15] and Shiles [32,33].

It is worth reminding that the β values from (i) and (ii) do not allow to model accurately the response of filters and mirrors containing Al [2,6,17,18]. Our new data are located in-between datasets (i) and (ii). For wavelengths below 41 nm, dataset (ii) (which corresponds to updated

Optics EXPRESS

values from Ref. 24) is in good agreement with our data up to 25 nm and then starts to deviate with values up to 14% lower than our data. For wavelengths longer than 41 nm, dataset (ii) is up to 37% lower than our data. Dataset (i) is 30 to 50% higher than our data in the entire spectral region 20–72 nm. The agreement between our β values from the regular and new (Σ) methods near 20 - 25 nm and the fact that the new method values remain in the center of the oscillatory patterns produced by the regular method in the entire spectral range from 20 to 72 nm, provide an additional validation of the significant improvement in accuracy of the new method β values, compared to the tabulated values from (i) and (ii).

The photoabsorption coefficients presented in this paper will be used in combination with measurements in other spectral ranges in order to calculate a new set of Al optical constants via Kramer-Krönig analyses. We believe that these new Al data will enable a much more accurate design and realization of EUV optical components in this spectral range.

5. Applicability of the new method to other materials

The method of determination of $Tmax(\lambda)$ and $Tmin(\lambda)$ described in the previous section is accurate as long as there are no high-frequency features in the absorption spectra that would be smoothed out by the interpolation. We do not expect any such high-frequency structures in the absorption spectra because, as is discussed in Section 2, the materials plotted in Fig. 1 (as well as most other materials) have no absorption edges in the region of applicability of this method. It is straightforward to verify this for any given material, in the event that an outermost absorption edge may exist in the vicinity of wavelengths where the new method is needed, such as, for example, the N2,3 edge of Zr (45.7 nm). In such cases, the new method should be applied in a wavelength region that begins at wavelengths slightly longer than the absorption edge, to avoid the discontinuity in absorption that may exist right at the edge. The "regular method" of Eq. (2) can then be applied for wavelengths right at the edge and shorter than the edge. Note that one can use the quality of the agreement between experimental data and Eq. (9) (i.e: the coefficient of determination) as an additional validation of the absence of high-frequency features in the absorption spectra. This is because the wavelength positions of the oscillation extrema, λ_i and λ_j, (see Section 4) are different for each sample because they depend on the thickness of the material. Thus, if any significant high-frequency features in $\beta(\lambda)$ existed, they would affect the interpolated $Tmax(\lambda)$ and $Tmin(\lambda)$ differently for each sample, which would result in a mis-alignment of the experimental data points plotted in Fig. 5 (b).

In general, the new Σ method of Eq. (9) is applicable to all materials that exhibit oscillations due to multiple reflections, in $T(\lambda)$. The amplitude of the oscillations caused by multiple reflections is determined by the value of $|f|$ (see Eq. (4)). In particular, the Σ method can be applied efficiently on all materials listed in Fig. 1, as well as other materials, which present values of $|f|$ that exceed 1 ± 0.025. The new Σ method remains valid in spectral regions where transmittance may vary rapidly and in a monotonic manner vs. wavelength, as shown in the case of Al in the wavelength region 20- 30 nm (see Figs. 3 and 4(b)). As explained above, the region of applicability of the Σ method includes, in general, wavelengths longer than the outermost electronic absorption edge of a given material. The new Σ method can be applied at wavelengths even longer than 80 nm, up to the onset of the plasma frequency region for metals, if one optimizes the material thicknesses, the capping layers and/or the light source flux. As has been demonstrated in Section 4, the new Σ method is consistent with and complementary to the regular method of Eq. (2), which has been employed at shorter wavelengths; in earlier work, the regular method has been shown to have exquisite spectral resolution and has captured extensive fine structure including sharp resonances, in the vicinity of numerous electronic absorption edges [25–29]. Therefore, the two transmittance-based methods (new Σ method and regular method) can be employed to provide accurate photoabsorption values in a wide spectral range, extending from the UV to the hard x-ray. As has been shown in this paper, one needs to fabricate thin enough freestanding samples

Optics EXPRESS

in order to measure transmittance at wavelengths longer than 20 nm. The method to produce freestanding thin films that we used for the Al samples in this manuscript has already been demonstrated for a large variety of thin film materials with thicknesses down to 20 nm [22–30] and is applicable to most materials of interest. For materials that cannot be made freestanding with a thin enough thickness (for example because of mechanical stress within the film), one can perform transmittance measurements on thin films deposited directly on photodiode detectors [31,39]. In that case, the vacuum exit medium in Fig. 2 is replaced by a solid exit medium (the photodiode), and equations similar to the ones in Section 2 can be derived.

6. Conclusion

We proposed a new method for the determination of EUV photoabsorption based on transmittance spectra of thin films, that circumvents the problem of multiple reflections. This method is particularly applicable for EUV wavelengths longer than 20 nm, where such reflections are pronounced and reliable refractive index values are very scarce. We demonstrated the new method on experimental transmittance data measured on different self-supported aluminum thin films and we derived a new set of photoabsorption coefficients from 20 nm to 72 nm wavelengths, for this material.

The new method should be used to determine accurate refractive index values for several other materials of interest for this wavelength range and extend the availability of accurate tabulated refractive index values to longer EUV wavelengths. This advance will allow the design and realization of efficient optical instrumentation in a spectral region that is crucial for lasers and high-harmonic sources, solar and planetary physics, astrophysics and semiconductor manufacturing.

This method is applicable at the longest EUV wavelengths, where most metals have their plasma frequency and can be used as an accurate experimental tool to validate atomic/molecular models.

Our approach can also be applied to films with an "infinite" solid on one side, as for example in the case of transmittance measurements of thin films deposited directly on photodiode detectors. In this manner, the usefulness of this method can be extended to an even larger variety of materials with thicknesses down to the atomic scale.

Funding. Lawrence Livermore National Laboratory (DE-AC52-07NA27344, LDRD project 20-FS-026); Lawrence Berkeley National Laboratory (DE-AC03-76F00098).

Acknowledgments. This work was performed under the auspices of the Institut d'Optique Graduate School, Université Paris-Saclay, and of the U.S. Department of Energy by Lawrence Livermore National Laboratory and by the University of California Lawrence Berkeley National Laboratory. The authors are thankful to Marie-Anne Descalle and Sonia Létant (LLNL) for support of this project and Jeff Robinson (LLNL) for technical assistance. The LLNL document release number is LLNL-JRNL-835251.

Disclosures. The authors declare no conflicts of interest.

Data availability. Data underlying the results presented in this paper are not publicly available at this time but may be obtained from the authors upon reasonable request.

References

1. M. Richter and G. Ulm, "Metrology with Synchrotron Radiation," in *Synchrotron Light Sources and Free-Electron Lasers*, E. Jaeschke, S. Khan, J. Schneider, and J. Hastings, eds. (Springer, 2020), pp 1575–1610.
2. P. Boerner, C. Edwards, and J. Lemen, *et al.*, "Initial Calibration of the Atmospheric Imaging Assembly (AIA) on the Solar Dynamics Observatory (SDO)," Sol. Phys. **275**(1-2), 41–66 (2012).
3. E.M. Gullikson, "Optical Properties of Materials," in *Vacuum Ultraviolet Spectroscopy*, J.A.R. Samson and D.L. Ederer, eds. (Academic Press, 2000), pp 257–270.
4. J. Seely, L. Goray, D. Windt, B. Kjornrattanawanich, Y. Uspenskii, and A. Vinogradov, "Extreme ultraviolet optical constants for the design and fabrication of multilayer-coated gratings," Proc. SPIE **5538**, 43–52 (2004).
5. B. Kjornrattanawanich, D. L. Windt, and J. F. Seely, "Normal- incidence silicon–gadolinium multilayers for imaging at 63 nm wavelength," Opt. Lett. **33**(9), 965–967 (2008).

Optics EXPRESS

6. J. Rebellato, R. Soufli, E. Meltchakov, E. Gullikson, S. de Rossi, and F. Delmotte, "High efficiency Al/Sc-based multilayer coatings in the EUV wavelength range above 40 nanometers," Opt. Lett. **45**(4), 869–872 (2020).
7. T. Helk, E. Berger, S. Jamnuch, L. Hoffmann, A. Kabacinski, J. Gautier, F. Tissandier, J.-P. Goddet, H.-T. Chang, J. Oh, C. D. Pemmaraju, T. A. Pascal, S. Sebban, C. Spielmann, and M. Zuerch, "Table-top extreme ultraviolet second harmonic generation," Sci. Adv. **7**(21), eabe2265 (2021).
8. S. Heinbuch, M. Grisham, D. Martz, and J. J. Rocca, "Demonstration of a desk-top size high repetition rate soft x-ray laser," Opt. Express **13**(11), 4050–4055 (2005).
9. Y. Oishi, M. Kaku, A. Suda, F. Kannari, and K. Midorikawa, "Generation of extreme ultraviolet continuum radiation driven by a sub-10-fs two-color field," Opt. Express **14**(16), 7230–7237 (2006).
10. B. De Pontieu, S. W. McIntosh, M. Carlsson, V. H. Hansteen, T. D. Tarbell, P. Boerner, J. Martinez-Sykora, C. J. Schrijver, and A. M. Title, "The Origins of Hot Plasma in the Solar Corona," Science **331**(6013), 55–58 (2011).
11. D. B. Seaton, J. M. Hughes, S. K. Tadikonda, A. Caspi, C. E. DeForest, A. Krimchansky, N. E. Hurlburt, R. Seguin, and G. Slater, "The Sun's dynamic extended corona observed in extreme ultraviolet," Nat Astron **5**(10), 1029–1035 (2021).
12. P. Rochus, F. Auchère, and D. Berghmans, *et al.*, "The Solar Orbiter EUI instrument: The Extreme Ultraviolet Imager," Astron. Astrophys. **642**, A8 (2020).
13. A. Corso and M. Pelizzo, "Extreme Ultraviolet Multilayer Nanostructures and Their Application to Solar Plasma Observations: A Review," J. Nanosci. Nanotechnol. **19**(1), 532–545 (2019).
14. B. Henke, E. Gullikson, and J. Davis, "X-ray interactions: Photoabsorption, scattering, transmission, and reflection at E 1⁄4 50–30000 eV, Z 1⁄4 1–92," At. Data Nucl. Data Tables **54**(2), 181–342 (1993).
15. Center for X-Ray Optics database: http://henke.lbl.gov/optical_constants/
16. N. Chkhalo, V. Polkovnikov, N. Salashchenko, M. Svechnikov, N. Tsybin, Y. Vainer, and S. Zuev, "Reflecting properties of narrowband Si/Al/Sc multilayer mirrors at 58.4 nm," Opt. Lett. **45**(17), 4666–4669 (2020).
17. M. Fernández-Perea, R. Soufli, J. C. Robinson, L. R. De Marcos, J. A. Méndez, J. I. Larruquert, and E. M. Gullikson, "Triple-wavelength, narrowband Mg/SiC multilayers with corrosion barriers and high peak reflectance in the 25-80 nm wavelength region," Opt. Express **20**(21), 24018–24029 (2012).
18. J. Rebellato, E. Meltchakov, R. Soufli, S. de Rossi, X. Zhang, F. Auchère, and F. Delmotte, "Analyses of tabulated optical constants for thin films in the EUV range and application to solar physics multilayer coatings," Proc. SPIE **10691**, 106911U (2018).
19. G. Horneck, N. Walter, and F. Westall, *et al.*, "AstRoMap European Astrobiology Roadmap," Astrobiology 16(3), 201–243 (2016) and https://www.nationalacademies.org/event/11-04-2021/pathways-to-discovery-in-astronomy-and-astrophysics-for-the-2020s-public-briefing
20. J. J. Drake, P. Cheimets, and C. Garraffo, *et al.*, "NExtUP: the Normal-incidence Extreme Ultraviolet Photometer," Proc. SPIE **11821**, 5 (2021).
21. K. France, B. Fleming, and A. Youngblood, *et al.*, "EUV spectroscopy with the ESCAPE mission: exploring the stellar drivers of exoplanet habitability," Proc. SPIE **11444**, 2 (2020).
22. R. W. Ditchburn and G. H. C. Freeman, "The optical constants of aluminium from 12 to 36 eV," Proc. R. Soc. Lond. A **294**(1436), 20–37 (1966).
23. R. Haensel, C. Kunz, T. Sasaki, and B. Sonntag, "Absorption Measurements of Copper, Silver, Tin, Gold, and Bismuth in the Far Ultraviolet," Appl. Opt. **7**(2), 301–306 (1968).
24. E. M. Gullikson, P. Denham, S. Mrowka, and J. H. Underwood, "Absolute photoabsorption measurements of Mg, Al, and Si in the soft-x-ray region below the L2,3 edges," Phys. Rev. B **49**(23), 16283–16288 (1994).
25. R. Soufli and E. M. Gullikson, "Absolute photoabsorption measurements of molybdenum in the range 60-930 eV for optical constant determination," Appl. Opt. **37**(10), 1713–1719 (1998).
26. R. Soufli, A. L. Aquila, F. Salmassi, M. Fernández-Perea, and E. M. Gullikson, "Optical constants of magnetron-sputtered boron carbide thin films from photoabsorption data in the range 30 to 770 eV," Appl. Opt. **47**(25), 4633–4639 (2008).
27. L. Rodríguez-de Marcos, J. I. Larruquert, M. Vidal-Dasilva, J. A. Aznárez, S. García-Cortés, J. A. Méndez, L. Poletto, F. Frassetto, A. M. Malvezzi, D. Bajoni, A. Giglia, N. Mahne, and S. Nannarone, "Transmittance and optical constants of Ca films in the 4–1000 eV spectral range," Appl. Opt. **54**(22), 6698 (2015).
28. F. Delmotte, J. Meyer-Ilse, F. Salmassi, R. Soufli, C. Burcklen, J. Rebellato, A. Jérome, I. Vickridge, E. Briand, and E. Gullikson, "Soft x-ray optical constants of sputtered chromium thin films with improved accuracy in the L and M absorption edge regions," J. Appl. Phys. **124**(3), 035107 (2018).
29. R. Soufli, F. Delmotte, J. Meyer-Ilse, F. Salmassi, N. Brejnholt, S. Masahi, D. Girou, F. Christensen, and E. Gullikson, "Optical constants of magnetron sputtered Pt thin films with improved accuracy in the N-and O-electronic shell absorption regions," J. Appl. Phys. **125**(8), 085106 (2019).
30. B. Kjornrattanawanich, D. L. Windt, J. A. Bellotti, and J. F. Seely, "Measurement of dysprosium optical constants in the 2-830 eV spectral range using a transmittance method, and compilation of the revised optical constants of lanthanum, terbium, neodymium, and gadolinium," Appl. Opt. **48**(16), 3084–3093 (2009).
31. Y. A. Uspenskii, J. F. Seely, N. L. Popov, A. V. Vinogradov, Y. P. Pershin, and V. V. Kondratenko, "Efficient method for the determination of extreme-ultraviolet optical constants in reactive materials: application to scandium and titanium," J. Opt. Soc. Am. A **21**(2), 298–305 (2004).

Optics EXPRESS

32. E. Shiles, T. Sasaki, M. Inokuti, and D. Y. Smith, "Self-consistency and sum-rule tests in the Kramers-Kronig analysis of optical data: Applications to aluminum," Phys. Rev. B **22**(4), 1612–1628 (1980).
33. 'Handbook of Optical Constants of Solids,' Edward D. Palik, ed. by Academic Press, Inc., 1985.
34. M. Vidal-Dasilva, A. L. Aquila, E. M. Gullikson, F. Salmassi, and J. I. Larruquert, "Optical constants of magnetron-sputtered magnesium films in the 25-1300 eV energy range," J. Appl. Phys. **108**(6), 063517 (2010).
35. A. Daude, A. Savary, G. Jezequel, and M. S. Robin, "« Determination des constantes optiques du magnesium entre 500 et 1400 Å »," Opt. Commun. **1**(5), 237–240 (1969).
36. M. Fernández-Perea, J. I. Larruquert, J. A. Aznárez, J. A. Méndez, L. Poletto, A. Marco Malvezzi, A. Giglia, and S. Nannarone, "Determination of optical constants of scandium films in the 20-1000 eV range," J. Opt. Soc. Am. A **23**(11), 2880–2887 (2006).
37. J. I. Larruquert, J. A. Aznárez, J. A. Méndez, A. Marco Malvezzi, L. Poletto, and S. Covini, "Optical properties of scandium films in the far and the extreme ultraviolet," Appl. Opt. **43**(16), 3271–3278 (2004).
38. D. L. Windt, W. C. Cash, M. Scott, P. Arendt, B. Newnam, R. F. Fisher, and A. B. Swartzlander, "Optical constants for thin films of Ti, Zr, Nb, Mo, Ru, Rh, Pd, Ag, Hf, Ta, W, Re, Ir, Os, Pt, and Au from 24 Å to 1216 Å," Appl. Opt. **27**(2), 246–278 (1988).
39. F. Seely, Y. A. Uspenskii, B. Kjornrattanawanich, and D. L. Windt, "Coated photodiode technique for the determination of the optical constants of reactive elements: La and Tb," Proc. SPIE **6317**, 63170T (2006).
40. W. R. Hunter, "Measurement of optical properties of materials in the vacuum ultraviolet spectral region," Appl. Opt. **21**(12), 2103–2114 (1982).
41. J. I. Larruquert, J. A. Méndez, and J. A. Aznárez, "Optical constants of aluminum films in the extreme ultraviolet interval of 82–77 nm," Appl. Opt. **35**(28), 5692–5697 (1996).
42. R. Soufli and E. M. Gullikson, "Reflectance measurements on clean surfaces for the determination of optical constants of silicon in the extreme ultraviolet–soft-x-ray region," Appl. Opt. **36**(22), 5499–5507 (1997).
43. C. Tarrio, R. N. Watts, T. B. Lucatorto, J. M. Slaughter, and C. M. Falco, "Optical constants of in situ-deposited films of important extreme-ultraviolet multilayer mirror materials," Appl. Opt. **37**(19), 4100–4104 (1998).
44. Q. Saadeh, P. Naujok, V. Philipsen, P. Hönicke, C. Laubis, C. Buchholz, A. Andrle, C. Stadelhoff, H. Mentzel, A. Schönstedt, V. Soltwisch, and F. Scholze, "Time-frequency analysis assisted determination of ruthenium optical constants in the sub-EUV spectral range 8 nm – 23.75 nm," Opt. Express **29**(25), 40993–41013 (2021).
45. C. Chang, E. Anderson, P. Naulleau, E. Gullikson, K. Goldberg, and D. Attwood, "Direct measurement of index of refraction in the extreme-ultraviolet wavelength region with a novel interferometer," Opt. Lett. **27**(12), 1028–1030 (2002).
46. G. S. M. Jansen, X. Liu, K. S. E. Eikema, and S. Witte, "Broadband extreme ultraviolet dispersion measurements using a high-harmonic source," Opt. Lett. **44**(15), 3625–3628 (2019).
47. R. Swanepoel, "Determination of the thickness and optical constants of amorphous silicon," J. Phys. E: Sci. Instrum. **16**(12), 1214–1222 (1983).
48. M. McClain, A. Feldman, D. Kahaner, and X. Ying, "An algorithm and computer program for the calculation of envelope curves," Comput. Phys. **5**(1), 45–48 (1991).